



PERGAMON

Aerosol Science 34 (2003) 1297–1321

Journal of
Aerosol Science

www.elsevier.com/locate/jaerosci

Coating of soot and $(\text{NH}_4)_2\text{SO}_4$ particles by ozonolysis products of α -pinene

H. Saathoff^{a,*}, K.-H. Naumann^a, M. Schnaiter^a, W. Schöck^a, O. Möhler^a,
U. Schurath^a, E. Weingartner^b, M. Gysel^b, U. Baltensperger^b

^a*Institute of Meteorology and Climate Research, Forschungszentrum Karlsruhe,
POB 3640, D-76021 Karlsruhe, Germany*

^b*Laboratory of Atmospheric Chemistry, Paul Scherrer Institut, 5232 Villigen, Switzerland*

Received 6 August 2002; accepted 7 January 2003

Abstract

The ozonolysis of α -pinene in a large aerosol chamber was used to generate secondary organic aerosol (SOA) mass by homogeneous nucleation, or by heterogeneous nucleation, either on soot, or on $(\text{NH}_4)_2\text{SO}_4$ seed aerosols. The rate of the α -pinene + ozone reaction and the aerosol yield of $\sim 19\%$ are in good agreement with literature data. The organic coating of soot particles leads to a compaction of the fractal agglomerates expressed by an increase in fractal dimension from 1.9 to 2.1 for Diesel soot, and from 2.0 to 2.3 for spark generated “Palas” soot. The dielectric coating of the soot particles with SOA layers between 2 to 11 nm gives rise to a substantial enhancement of their single scattering albedo, from about 0.2 to 0.5, and increases the effective absorption coefficients of both soot types by ca. 30%. The coating of both soot types increases the hygroscopic growth factors (HGF) to values close below the HGF measured for pure SOA material $d/d_0 \sim 1.12$ at 90% RH.

© 2003 Elsevier Ltd. All rights reserved.

Keywords: Aerosol coating; Secondary organic aerosol; Optical and hygroscopic properties

1. Introduction

Non-methane volatile organic compounds (NMVOC) are emitted in large quantities from vegetation. Total annual global emissions of biogenic volatile organic compounds (BVOC) are estimated to range from 491 to 1150 Tg C (Mueller, 1992; Fehsenfeld et al., 1992; Guenther et al., 1995). Isoprene (C_5H_8), monoterpenes ($\text{C}_{10}\text{H}_{16}$), and sesquiterpenes ($\text{C}_{15}\text{H}_{24}$) comprise the majority of these emissions. The reactions of monoterpenes and sesquiterpenes with OH, O_3 , and NO_3 yield secondary

* Corresponding author. Tel.: +49-7247-82-2897; fax: +49-7247-82-4332.

E-mail address: harald.saathoff@imk.fzk.de (H. Saathoff).

organic aerosol (SOA) mass in highly variable yields. SOA is believed to make up a large fraction of the aerosol over tropical continental regions (Andreae & Crutzen, 1997). For most terpenes, nighttime oxidation by ozone produces significantly higher aerosol yields than the photooxidation at daytime, which is dominated by reactions with OH radicals (Hoffmann et al., 1997; Griffin, Cocker III, Flagan, & Seinfeld, 1999a). While Andreae and Crutzen (1997) estimated that the global BVOC-derived SOA mass ranges between 30 to 270 Tg/yr, more recent estimates have narrowed this range down to 13–24 Tg/yr (Griffin, Cocker III, Seinfeld, & Dabdub, 1999b) and to 61–79 Tg/yr (Kanakidou, Tsigaridis, Dentener, & Crutzen, 2000). The dominant SOA forming compounds are monoterpenes of which α -pinene is the most abundant (Geron, Rasmussen, Arnts, & Guenther, 2000). Therefore the oxidation of α -pinene has been subject of many recent studies, making it one of the best investigated terpenes. Rate constants for the reactions of OH, O₃ and NO₃ with α -pinene (Atkinson, 1997; Aschmann, Reissell, Atkinson, & Arey, 1998; Khamaganov & Hites, 2001), the products of the reactions (Alvarado, Tuazon, Aschmann, Atkinson, & Arey, 1998; Christoffersen et al., 1998; Calogirou, Larsen, & Kotzias, 1999; Glasius et al., 2000; Yu, Cocker III, Griffin, Flagan, & Seinfeld, 1999; Kückelmann, Warscheid, & Hoffmann, 2000; Koch et al., 2000), and their SOA yields (Hatakeyama, Izumi, Fukuyama, & Akimoto, 1989; Odum et al., 1996; Hoffmann et al., 1997; Hoffmann, Bandur, Marggraf, & Linscheid, 1998; Griffin et al., 1999a; Kamens, Jang, Chien, & Leach, 1999) have been studied intensively, and have led to the development of models describing the formation of SOA (Barthelmie & Pryor, 1999; Jenkin, Schallcross, & Harvey, 2000; Pankow, Seinfeld, Asher, & Erdakos, 2001; Seinfeld, Erdakos, Asher, & Pankow, 2001). The ozonolysis of α -pinene is supposed to be one of the major atmospheric sources of SOA. To our knowledge only one other study (Leach, Kamens, Strommen, & Jang, 1999) has been done so far in which soot particles were coated with products of the α -pinene ozonolysis. That study focussed on the gas to particle partitioning of semi-volatile organic compounds using soot and SOA from the α -pinene + ozone reaction as particle phases.

Organics influence the interaction of aerosols with water vapour in the atmosphere (Novakov & Penner, 1993; Saxena, Hildemann, McMurry, & Seinfeld, 1995; Shulman, Jacobson, Charlson, Synovec, & Young, 1996). E.g., an organic coating on relatively hydrophobic soot aerosol particles may make them less hydrophobic, thus enhancing their ability to act as cloud condensation nuclei (CCN). Furthermore the optical properties of internally mixed black carbon and non-absorbing (e.g. organic carbon) aerosol particles differ from those of their external mixtures. They depend mainly on the source and the ageing of initially emitted soot particles (Liousse, Cachier, & Jennings, 1993; Liousse, Devaux, Dulac, & Cachier, 1995; Liousse et al., 1996). For example, the coating of soot particles with (NH₄)₂SO₄ is supposed to increase their effective mass absorption coefficient significantly (Fuller, Malm, & Kreidenweis, 1999).

The aim of the organic coating experiments during the AIDA soot characterisation campaign 1999 was to study the impact of organic coatings on the structure, the optical properties, and the hygroscopic properties of the seed particles. We chose the ozonolysis of α -pinene as a source of SOA because of its atmospheric relevance, and because this is one of the best investigated systems so far.

2. Experimental and modelling

The AIDA aerosol chamber and its instrumentation are described in two companion papers (Saathoff et al., 2003a; Schnaiter et al., 2003). The coating experiments were done always in the

following sequence: First, the chamber was filled with particle-free humidified synthetic air ($\sim 45\%$ relative humidity (RH) at 297 K); second, soot or ammonium sulphate aerosol was filled into the chamber using either two graphite spark generators (GfG 1000, Palas), a 4 cylinder turbo Diesel engine (TDI), or an ultrasonic nebulizer (GA 2400, Sinaptec) using a 0.09 M $(\text{NH}_4)_2\text{SO}_4$ solution; third, the seed aerosol was characterised; fourth, the particles were coated in situ by reacting α -pinene with a large excess of ozone. Fifth, the coated aerosol was characterised as described in the following paragraph.

Number concentrations of particles larger than 7 nm were measured continuously with two condensation particle counters (CPC 3022A, TSI) and size distributions were measured with a scanning mobility particle sizer (DMA 3071 & CPC 3010, TSI). Samples for total carbon/elemental carbon analysis were collected on preheated quartz fibre filters (Ø 47 mm, MK 360, Munktell / Ø 25 mm, Schleicher & Schüll), and were analysed with coulometric technique (TC) (Coulomat 702, Ströhlein) and a thermal method (Lavanchy et al., 1999). Aerosol extinction was determined periodically at 473 nm by means of an external White type optical cell (75 m folded path length, sensitivity $\sim 10^{-5} \text{ m}^{-1}$). The cell was run in series with a 5 m long optical flow tube which covered the spectral range 230–1000 nm at 2.5 nm spectral resolution (sensitivity $\sim 10^{-4} \text{ m}^{-1}$), and with an integrating nephelometer (3563, TSI) which yielded scattering and backscatter parameters at 450, 550, and 700 nm (Schnaiter et al., 2003). Absorption coefficients were determined by analysing filter samples with the integrating plate method (Horvath, 1997). The photoelectron emission charging (222 nm) of soot particles was measured with a photoelectric aerosol sensor (PAS 2000, EcoChem; Burtscher, 1992; Burtscher & Siegmann, 1994). This method is highly sensitive to the state of the surface, for example to material adsorbed on the particle surface. A number of studies have shown that ambient particles originating from incomplete combustion of hydrocarbons exhibit the highest photoelectric yield and may, therefore, be selectively detected. For details see Baltensperger, Weingartner, Burtscher, and Keskinen, 2001. The active surface area of soot particles was measured with a diffusion charger (LQ1-DC, Matter Engineering AG). This instrument uses a corona discharge to generate ions in the carrier gas. The ions attach to the surface of the particles which are collected in an electrically insulated filter (Matter, Siegmann, & Burtscher, 1999; Baltensperger et al., 2001). The structure of the aerosol particles which had been collected on polycarbonate filters (47 mm, Nuclepore, type 111106, Corning), were visualised by Scanning Electron Microscopy (SEM, JSM-840, Jeol). The hygroscopic properties of the aerosol were measured with a hygroscopicity tandem differential mobility analyser (HTDMA) (Weingartner, Gysel, & Baltensperger, 2002). Briefly, in this instrument, the aerosol is first dried to a low relative humidity ($\text{RH} < 5\%$) and fed into the first differential mobility analyzer (DMA) where particles of a certain “dry” size are selected ($d = d_0$). After exposure to higher RH (typically $\text{RH} = 85\text{--}90\%$), the new particle size distribution is determined with a second DMA combined with a condensation particle counter (CPC), and hygroscopic growth factors (HGF, d/d_0), defined as the ratio of the humidified diameter d to the dry diameter d_0 , are deduced. To ensure a constant temperature within the entire HTDMA system, both DMAs as well as the humidifier are submersed in a water bath at $T = 19^\circ\text{C}$. The applied SMPS technique enabled a precise measurement of the growth factors with a time resolution of 5 min.

After characterising the seed aerosol in the AIDA chamber, about 500 ppb ozone and subsequently (61 ± 3) ppb α -pinene were added by evaporating (5.1 ± 0.2) hPa α -pinene (99%, Aldrich) into a 1-liter glass bulb, and flushing the contents into the chamber with 10 SLM synthetic air for 3 min. The end of the flushing procedure marked $t=0$ on the relative time scale of this series of experiments.

Ozone was generated with a silent discharge generator (Semozon 030.2, Sorbios) in pure oxygen (99.999%, Messer Griesheim). The concentrations of α -pinene, sulfate aerosol, ozone, and SF₆ which had been added as an inert dilution tracer were measured by long path FTIR spectrometry (Bruker IFS 66v, 254 m folded optical path, spectral range 4000–800 cm⁻¹, resolution 0.125 cm⁻¹). These determinations were complemented by discontinuous *ex situ* measurements with a commercial ozone monitor (Environment O₃–41M).

The reaction of ozone with α -pinene yields products with very low vapour pressures like pinic acid, pinonic acid, hydroxy pinonaldehyde, and other oxygenated compounds (Yu et al., 1999). These can either condense on seed particles, or form new particles by homogeneous nucleation, or both, depending on the rate of product formation and the surface area density of the seed aerosol. The experimental data were analysed with an updated version of the aerosol physico-chemical simulation code COSIMA (Naumann & Bunz, 1992; Naumann, 2003) which accounts for the dynamics of fractal particles, their optical properties, and homogeneous as well as heterogeneous chemistry in the aerosol chamber. In the current version a constant volume fractal dimension D of the soot particles had to be assumed. Therefore, a detailed dynamical modelling of the restructuring process induced by the organic coating was not yet possible. However, an improved version of the COSIMA code is under development, which will allow the volume fractal dimension D to be treated as a time-dependent function.

3. Results and discussion

The following results pertain to experiments No. 6–10 of the soot characterisation campaign (cf. Table 3 of Saathoff et al., 2003a). The initial ozone concentration at $t = 0$ was 500 ppb in all experiments except in experiment No. 7 where it was 385 ppb. The temperatures during these experiments ranged from 296.1 to 297.6 K. The rate constant of the reaction O₃ + α -pinene \rightarrow products is 8.6×10^{-17} cm³molecule⁻¹ s⁻¹ at 298 K (Atkinson, 1997). Since ozone was always in large excess, the α -pinene concentrations were observed to decrease nearly exponentially with half-lives in the order of 10 min. The known or estimated properties of the seed aerosols used in the following experiments as well as their modifications caused by the *in situ* ozonolysis of 61 ppb α -pinene are listed in Table 1.

3.1. New particle formation in the absence of seed aerosol

During experiment No. 10 500 ppb ozone were added to particle-free humidified synthetic air in the AIDA chamber 36 min prior to the injection of α -pinene. Reactions of ozone with unknown impurities gave rise to the formation of 10⁵ cm⁻³ very small particles, cf. Fig. 1, which eventually grew into the detectable size range of the scanning mobility particle sizer (SMPS) (15–763 nm). The volume and surface area concentrations of these particles were negligible. After the addition of 61 ppb α -pinene the particle number concentration increased rapidly to almost 2×10^5 cm⁻³, and a nucleation mode at about 60 nm mobility equivalent diameter was formed, cf. Figs. 1 and 2. The particles grew subsequently to diameters of about 110 nm forming a bi-modal size distribution due to coagulation and the ongoing heterogeneous nucleation. The particle surface area and volume which were calculated from the measured number size distributions passed through maximum values of

Table 1
Aerosol surface and coating estimates

Experiment No.	10	8	7	9
Seed aerosol type	none	(NH ₄) ₂ SO ₄	Diesel soot	“Palas” soot
Initial carbon mass concn. (μg m ⁻³)	—	710 ± 70	78 ± 23	111 ± 34
Specific surface area (m ² g ⁻¹)	—	3	91 ^a	(310 ± 30) ^b
Active specific surface area (m ² g ⁻¹)	—	3	60 ^c	150 ^c
Initial surface area concn. (cm ² m ⁻³)	—	22 ± 4	(47–71) ^d	(167–342) ^d
SOA volume concn. (cm ³ m ⁻³)	6.5 × 10 ⁻⁵	6.8 × 10 ⁻⁵	~6.5 × 10 ⁻⁵	~6.5 × 10 ⁻⁵
Formed SOA mass (μg m ⁻³)	65	68	~ 65	~ 65
<i>m</i> _{cond.} /(<i>m</i> _{nucl.} + <i>m</i> _{cond.})	1.0	~ 0.8	~ 0.8	~ 1.0
Coating thickness ^e (nm)	—	25 ± 13	7–11	2–4
Coating thickness (HTDMA) ^f (nm)	—	10 ± 4	—	—

^aNIST Standard reference material 2975 (2000).

^bKuznetsov et al. (2003).

^cNaumann (2003); Xiong, Pratsinis, and Weimer (1992).

^dBased on Fuchs and BET surface area, respectively.

^eCondensed SOA volume/initial surface area.

^fFor *d*₀ = 200 nm particles.

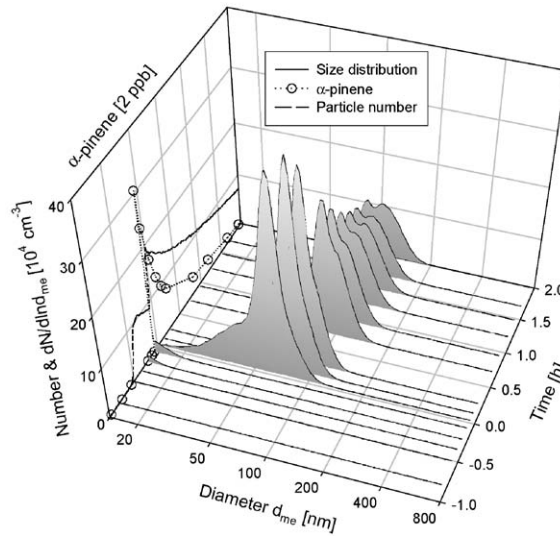


Fig. 1. Evolution of the size distribution and number concentration of the pure organic aerosol formed upon ozonolysis of α -pinene without seed aerosol in experiment No. 10.

(35 ± 7) cm² m⁻³ about 20 min after the addition of α -pinene, and of (5.8 ± 1.7) × 10⁻⁵ cm³ m⁻³ about 20 min later. Fitting the measured aerosol volume *V* with the function $V = V^{\circ} \times (a/(b - a)) \times (e^{-at} - e^{-bt})$ leads to an estimate of the formed aerosol volume of 65 × 10⁻⁶ cm³ m⁻³. The losses of potential SOA material to the chamber wall can be neglected since the pseudo first order rate of

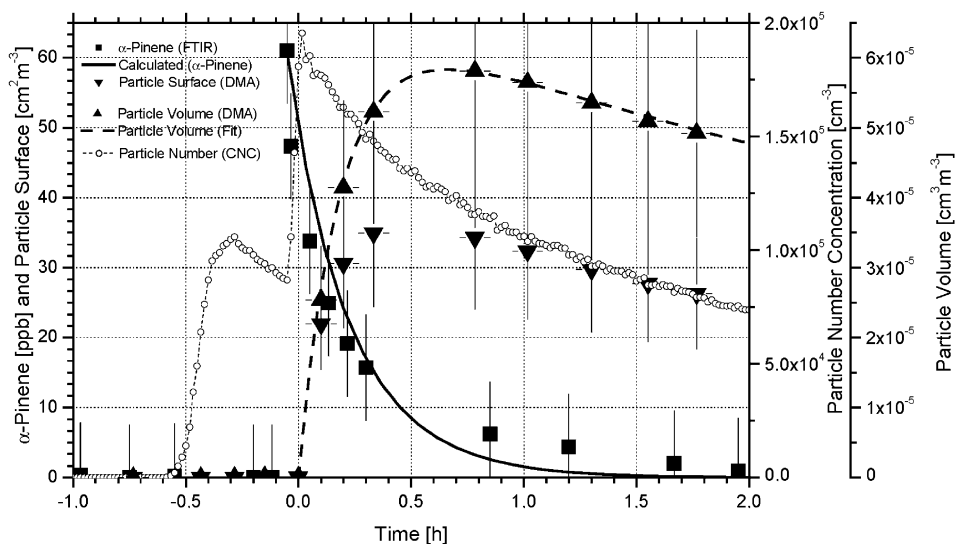


Fig. 2. Evolution of the aerosol volume calculated from the measured size distribution during experiment No. 10. Additionally the evolution of the number concentration and the depletion of the α -pinene concentration are shown.

SOA mass formation of about $1/a = 1.4 \times 10^{-3} \text{ s}^{-1}$ is much faster than the upper limit of the wall loss rate for a typical SOA molecule (185 g mol^{-1} ; 500 pm diameter) of 10^{-4} s^{-1} . This limiting wall loss rate was estimated from the value measured for N_2O_5 , a species exhibiting a high sticking probability, by adjusting the molecular mass while assuming diffusion controlled conditions. The density ρ of the SOA material can be estimated by comparison with compounds such as pinic acid diethyl ester ($\rho = 1.0104 \text{ g cm}^{-3}$), cyclopropanedicarboxylic acid diethyl ester ($\rho = 1.062 \text{ g cm}^{-3}$), or octanedionic acid diethyl ester ($\rho = 0.9811 \text{ g cm}^{-3}$) (Lide, 1999) to be in the order of 1 g cm^{-3} . This implies a SOA yield of about $65 \mu\text{g m}^{-3}$. The fractional aerosol yield Y was defined by Odum et al. (1996) as the fraction of the reactive organic gas (here α -pinene) that is converted to aerosol: $Y = \Delta M_{\text{aerosol}} / \Delta M_{\alpha\text{-pinene}}$. Compared to the reacted amount of $61 \text{ ppb} = 343 \mu\text{g m}^{-3}$ α -pinene the $65 \mu\text{g m}^{-3}$ of SOA correspond to an aerosol yield of about 19%, in good agreement with Griffin et al. (1999a) and Yu et al. (1999). However, the temperature in their experiments (308 K) was about 10 K higher. A 10 K decrease in temperature is estimated to increase SOA yields by 20–150%, depending on the assumed evaporation enthalpy (Sheehan & Bowman, 2001). The good agreement with our data may be explained by the fact that Griffin et al. (1999a) measured the size distributions at about 298 K , thus comparable to our conditions. According to Seinfeld et al. (2001) and Cocker, Clegg, Flagan, and Seinfeld (2001) the RH used in our experiments (43–35%) should have only a small effect on the SOA yield and thus it should be comparable to the results of Griffin et al. (1999a) obtained at 10% RH.

Assuming an average carbon content of 64% of the formed organic aerosol (calculated using the particle composition given by Jenkin et al. (2000)), about $42 \mu\text{g m}^{-3}$ of particulate carbon were formed. This is much less than the carbon yield calculated from the coulometric analysis of quartz filter samples of $(85 \pm 26) \mu\text{g m}^{-3}$ right after the nucleation event, and of $(49 \pm 15) \mu\text{g m}^{-3}$ 12 h later (Saathoff et al., 2003b). The large discrepancy is attributed to the adsorption of semi-volatile

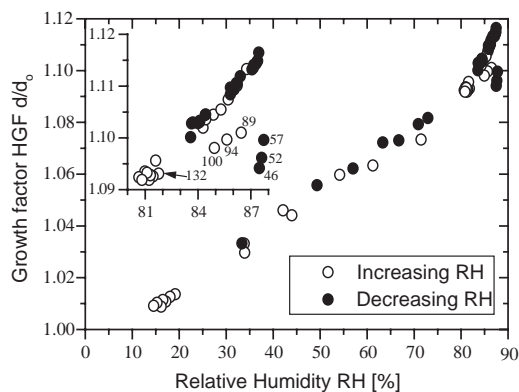


Fig. 3. Humidogram of SOA particles (dry diameter $d_0 = 100$ nm) produced by ozonolysis of α -pinene. The inset shows a magnification of the upper RH range and the numbers next to the points denote the ageing time (in minutes) after the addition of α -pinene.

ozonolysis products on the quartz fiber filters, which are included in the total carbon determination although they do not contribute to the SOA mass.

The optical properties of the formed SOA in the 230–1000 nm range are discussed by Schnaiter et al. (2003). A single scattering albedo of 1 was found for the visible spectral region, reflecting the non-absorbing nature of the SOA. FTIR spectra of the SOA could not be recorded due to the strong water vapour bands in the spectral range where carboxylic acid functionalities are expected to absorb.

The hygroscopic properties of size-selected SOA particles were measured with the HTDMA operating at $RH \leq 85\%$. In this experiment the RH in the second DMA was continuously changed which allowed measuring humidograms for decreasing and increasing RH conditions. (see Weingartner et al., 2002 for more information). No broadening of the monodisperse size distribution during water uptake was observed, indicating an internally mixed SOA aerosol with homogeneous hygroscopic properties. Fig. 3 shows that the $d_0 = 100$ nm particles were characterised by a continuous increase of the HGF with increasing RH. This is in good agreement with the picture of SOA particles consisting of supercooled liquid organic solutions. A clear absence of efflorescence (for $RH > 10\%$) was also observed in a field campaign (Weingartner et al., 2002) where the hygroscopic properties of aged free tropospheric particles were investigated. Whether the absence of efflorescence of the free tropospheric aerosol is caused by organic components or by a mixture effect only is still an open question. However, since no efflorescence was observed for pure SOA particles, SOA might contribute to a distinct reduction of efflorescence RH of atmospheric particles.

It is clearly seen in the inset of Fig. 3 that in the early stage of SOA formation the SOA particles showed increasing hygroscopicity with increasing residence time t in the chamber. Freshly produced particles with $t < \sim 2$ h were characterised by significantly lower HGF than the aged particles, indicating that the composition of the SOA particles varies during the first two hours of α -pinene oxidation. At $t = 6$ h, a $HGF = 1.106 \pm 0.002$ (for $d_0 = 100$ nm and $RH = 85\%$) was measured, which remained constant to the end ($t = 12$ h) of the experiment. Particles with $d_0 = 200$ nm which appeared at $t > \sim 4$ h exhibited the same HGF (not shown in Fig. 3). Overall, the measured HGF values are

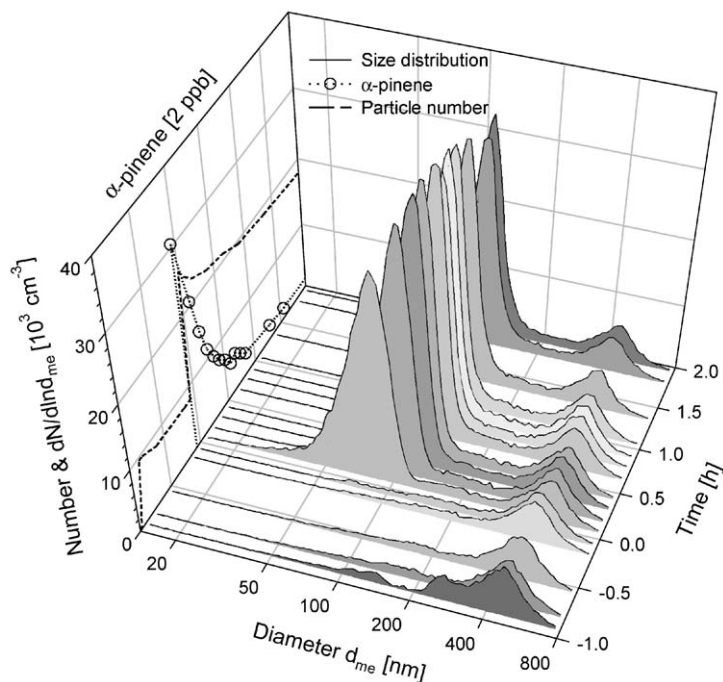


Fig. 4. Evolution of the size distribution and number concentration of $(\text{NH}_4)_2\text{SO}_4$ and organic aerosol formed upon ozonolysis of α -pinene in experiment No. 8.

in fairly good agreement with measurements performed at an outdoor smog chamber ($\sim 200 \text{ m}^3$) in Valencia, where SOA particles with $d_0 = 50\text{--}120 \text{ nm}$ produced by ozonolysis of α -pinene experienced an average HGF of 1.070 ± 0.002 at 84.1 % RH (Virkkula, Van Dingenen, Raes, & Hjorth, 1999).

3.2. Coating of $(\text{NH}_4)_2\text{SO}_4$ aerosol particles

Experiment No. 8 was done in the same way as experiment No. 10 except that about $710 \mu\text{g m}^{-3}$ $(\text{NH}_4)_2\text{SO}_4$ seed aerosol was present when the reaction of α -pinene with ozone occurred. Fig. 4 shows the initial $(\text{NH}_4)_2\text{SO}_4$ size distribution with a peak at 450 nm. As can be seen in Figs. 4 and 5 the particle number concentration increased rapidly from 8×10^3 to $2.6 \times 10^4 \text{ cm}^{-3}$ when 61 ppb α -pinene were added, and a nucleation mode at about 80 nm was formed. This shows that new particle formation was not completely suppressed by the seed aerosol, although an order of magnitude less new particles were formed than in the absence of seed particles. The peak of the nucleation mode shifted eventually from 80 to 110 nm. Furthermore, the peak of the $(\text{NH}_4)_2\text{SO}_4$ mode shifted from 450 to 480 nm due to condensation of SOA mass on the seed particles, which dominate the available surface area in spite of the larger number density of the nucleation mode particles. Integration of the volume distribution reveals that about 82% of the formed aerosol volume condensed on the seed aerosol. Fig. 5 shows the evolution of the aerosol volume during this coating experiment. From this plot we can estimate (see above) that about $6.8 \times 10^{-5} \text{ cm}^3 \text{ m}^{-3}$ ($68 \mu\text{g m}^{-3}$) of SOA were formed, which is in good agreement with experiment No. 10 (cf. Table 1). Before

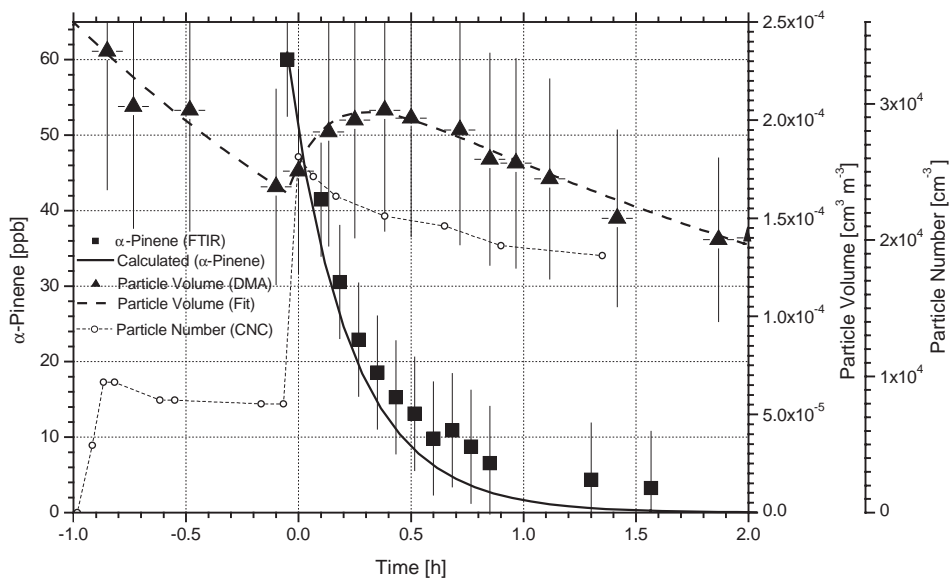


Fig. 5. Evolution of the aerosol volume calculated from the measured size distribution during experiment No. 8. Additionally the evolution of the number concentration and the depletion of the α -pinene concentration are shown.

the coating process started the seed aerosol surface area density was calculated from the measured number size distribution to $(22 \pm 4) \text{ cm}^2 \text{ m}^{-3}$. Distributing the SOA volume homogeneously over this surface leads to an average coating thickness of about $(25 \pm 13) \text{ nm}$. The error was estimated using an uncertainty for the SOA volume of $\sim 30\%$.

Fig. 6a shows the temporal evolution of the measured HGF during this experiment where, in contrast to the former experiment, the RH was kept constant at $\sim 90.5\%$. At $t < 0$ the uncoated $d_0 = 100$ and 200 nm $(\text{NH}_4)_2\text{SO}_4$ particles experienced a HGF = 1.56 and 1.65, respectively at RH = 90.5%. The values at $d_0 = 100 \text{ nm}$ are by $\sim 7\%$ lower than the ones reported by Gysel, Weingartner, and Baltensperger (2002), which may be due to an unknown contamination of the small $(\text{NH}_4)_2\text{SO}_4$ particles. The measured HGF for freshly emitted $(\text{NH}_4)_2\text{SO}_4$ particles at $d_0 = 200 \text{ nm}$ agree well with theory. After the coating the formerly monomodal growth distribution of the $d_0 = 100 \text{ nm}$ particles transformed into a distinctly bimodal growth distribution, and the two modes are referred to as less and more hygroscopic modes (LHM and MHM). For $d_0 = 200 \text{ nm}$ particles the growth distributions remained monomodal, i.e. only a more hygroscopic mode was present. This difference can be explained as follows: The nucleation mode particles remained mainly smaller than $d_0 = 200 \text{ nm}$, and therefore no external mixture is seen in this size channel. For $d_0 < 200 \text{ nm}$ the coating leads to mixed more hygroscopic $(\text{NH}_4)_2\text{SO}_4/\text{SOA}$ particles which are externally mixed with less hygroscopic “pure” SOA nucleation mode particles. As already seen in experiment 10 an increase in hygroscopic growth of the SOA particles (LHM, $d_0 = 100 \text{ nm}$) was observed mainly within the first 1–2 h after starting the α -pinene oxidation. At $t = 6 \text{ h}$ a HGF of $d/d_0 = 1.121$ at RH = 90.3% was measured, which agrees well with SOA particle hygroscopicity from Experiment 10 (Fig. 3).

Since HGFs are known for pure SOA particles as well as for the uncoated $(\text{NH}_4)_2\text{SO}_4$ particles and the coated $(\text{NH}_4)_2\text{SO}_4$ particles, one can estimate the volume fraction of the organic coating.

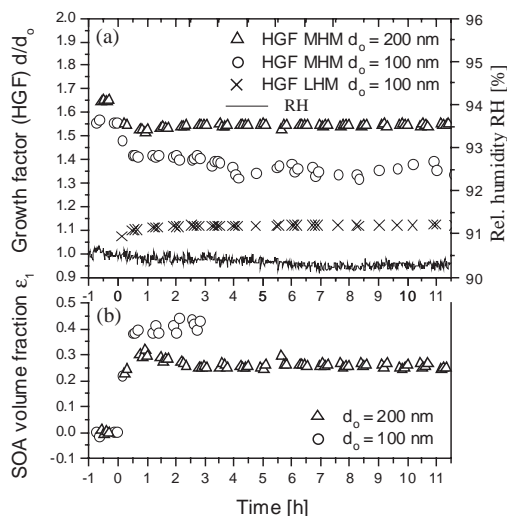


Fig. 6. Temporal evolution of the measured hygroscopic growth factor (HGF) of $d_0 = 100$ nm and 200 nm for the less and more hygroscopic modes (LHM and MHM) during experiment No. 8 for a RH of $\sim 90.5\%$ (a). Evolution of the calculated SOA volume fraction (b).

Assuming spherical particles and independent additive hygroscopic behaviour of the different components in the mixed particle the volume V of a coated particle at a certain RH is given by

$$V = Gf_1^3 V_1 + Gf_2^3 V_2, \quad (1)$$

where the subscripts 1 and 2 stand for the “pure” SOA and $(\text{NH}_4)_2\text{SO}_4$ material, V_1 and V_2 are the corresponding dry volumes, and Gf_1 and Gf_2 the growth factors of the individual substances. From this it follows that the SOA volume fraction ε_1 in the coated particles is given by

$$\varepsilon_1 = \frac{Gf_2^3 - Gf_{\text{mix}}^3}{Gf_2^3 - Gf_1^3}, \quad (2)$$

where Gf_{mix} denotes the growth factor of the coated particles. Volume fractions ε_1 calculated with Eq. (2) are shown in Fig. 6b for particles with $d_0 = 100$ and 200 nm. Gf_1 ($d_0 = 100$ nm) is used for particles with $d_0 = 200$ nm also, since no large SOA particles were observed in Experiment 8. Two hours after the addition of α -pinene the estimated SOA volume fractions for $d_0 = 100$ and 200 nm particles are $\varepsilon_1 = 41 \pm 8$ and $28 \pm 10\%$, respectively. These uncertainties were calculated by error propagation from the uncertainty of the measured growth factors. Dividing the SOA yield by the initial $(\text{NH}_4)_2\text{SO}_4$ mass concentration (see Table 1), gives an upper limit for the average SOA mass fraction of $\sim 10\%$. The volume fractions of $\varepsilon_1 = 41 \pm 8$ and $28 \pm 10\%$ corresponds to a SOA mass fraction of 28 ± 5 and $18 \pm 6\%$ for 100 and 200 nm particles, respectively, assuming a SOA density of 1 g cm^{-3} . This is not inconsistent because particles larger than 400 nm in diameter give the main contribution to the aerosol mass, and the condensed volume fraction decreases with increasing particle size. The estimated SOA volume fractions correspond to coating thickness of 8 ± 2 and 10 ± 4 nm for 100 and 200 nm particles, respectively. (see Table 1). The difference to the average value of 25 ± 13 nm (see Table 1) may arise from the fact that the hygroscopicity measurement

was done on the edge of the coated particle size mode and from the inaccuracy of the model assumption (independent additive behaviour). Indeed, strong interactions in binary inorganic-organic (e.g. $(\text{NH}_4)_2\text{SO}_4$ with pinonic acid which is a typical product of α -pinene-ozone reactions, see above) particles were observed in recent studies using the HTDMA (Cruz & Pandis, 2000), and the electrodynamic balance technique (Choi & Chan, 2002). Especially for $(\text{NH}_4)_2\text{SO}_4$ -organic acid mixtures experimental hygroscopic growth factors were often larger than the theoretical value based on the assumption of independent additive behaviour. Such a positive interaction may also be the reason for the underestimation of the coating thickness in this experiment.

Open questions are the effects of organic compounds on the efflorescence (ERH) and deliquescence relative humidity (DRH) of mixed inorganic-organic particles. Various phenomena have been reported by Cruz et al. (2000), Lightstone et al. (2000), and Choi and Chan (2002). At the end of this experiment ($t > 12$ h) the RH dependence of the HGFs under increasing RH conditions was investigated. Observed HGFs ($d_0 = 200$ nm) were smaller than 1.03 for $\text{RH} < 70\%$, i.e. the $(\text{NH}_4)_2\text{SO}_4$ remained solid and the small water uptake is attributed to the hygroscopic growth of the SOA coating. At $\text{RH} \geq 80\%$ coated particles were completely deliquescent similar to pure $(\text{NH}_4)_2\text{SO}_4$ particles ($\text{DRH} = 80\%$, Gysel et al., 2002). Although in the RH range $70\% < \text{RH} < 80\%$ no measurements of HGFs are available one can still conclude that a possible reduction of the DRH by the organic coating is smaller than 10%. The effect of the organic coating on the ERH was not investigated.

3.3. Coating of diesel soot aerosol particles

In experiment No. 7 (78 ± 23) $\mu\text{g C m}^{-3}$ Diesel soot and 385 ppb ozone were present in the AIDA chamber when 61 ppb α -pinene were added. Three hours of prior interaction with initially 500 ppb ozone had changed the surface properties of the Diesel soot particles significantly, as evidenced by the increase of oxygen-containing hydrocarbon fragments in the particle mass spectra which are presented in the companion paper of Kirchner et al. (2003). The change in surface properties caused a decrease of the photoemission signal from 2200 to 650 fA. However, the influence of the ozone soot interaction on the hygroscopic and optical properties of the Diesel soot particles was negligible.

Diesel soot aerosol offers a significantly larger specific surface area than the ammonium sulphate seed aerosol of experiment No. 8. Typical Diesel exhaust particles have specific surface areas of about $100 \text{ m}^2 \text{ g}^{-1}$ (Kittelson, 1998). For example, the standard reference material 2975 (Diesel particulate matter) of the National Institute of Standards & Technology (NIST) has a certified specific surface area of $91 \text{ m}^2 \text{ g}^{-1}$ determined by N_2 adsorption (BET method). However, this specific surface area must be clearly distinguished from the active surface area which is measured by the diffusion charger. To take this into account we used the measured size distribution and mass concentration of the seed aerosol as input for the COSIMA model (Naumann, 2003) and calculated the accessible or active surface area of Diesel soot to $60 \text{ m}^2 \text{ g}^{-1}$ (cf. Table 1). Comparing this value with the signal of the diffusion charger led to a calibration factor of $\sim 5.2 \times 10^{-7} \text{ cm}^2 \text{ cm}^{-3} \text{ fA}^{-1}$ for Diesel soot aerosol.

As evidenced in Fig. 7, dramatic changes in most of the measured aerosol parameters occurred when α -pinene was added to the Diesel soot–ozone mixture. Besides new particle formation a significant amount of oxidation products of α -pinene must have condensed on the Diesel soot particles. This is concluded from the fact that the volume density of the nucleation mode of $(12 \pm 6) \times 10^{-6} \text{ cm}^3 \text{ m}^{-3}$

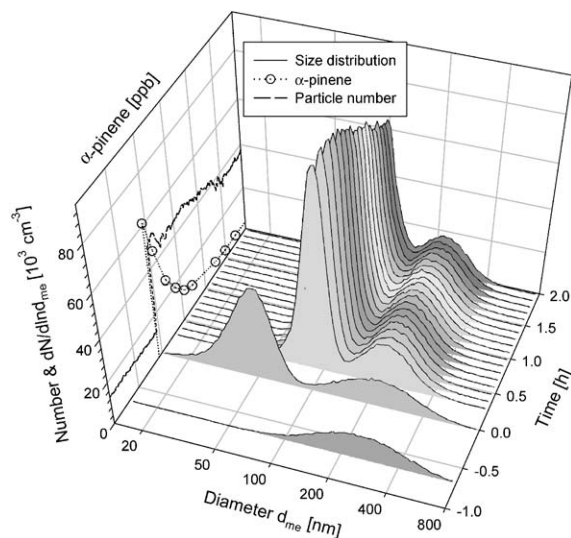


Fig. 7. Evolution of the size distribution and number concentration of Diesel soot and organic aerosol formed upon ozonolysis of α -pinene in experiment No. 7.

accounted for only about 18% of the expected SOA yield of $65 \times 10^{-6} \text{ cm}^3 \text{ m}^{-3}$ (assumed to be similar as in the two reference experiments Nos. 8 and 10), and is in sharp contrast to the observed shift of the Diesel soot mode from 245 to 222 nm after the coating event. The decrease of the mobility equivalent particle diameter results from the compaction of the fractal soot agglomerates, due to capillary forces exerted by the SOA which forms a supercooled liquid coating. The compaction is confirmed by electron micrographs of particles collected before and after the coating event (Fig. 8) and by the significant narrowing of the Diesel particle mode (Fig. 7): the mode width decreased from $\sigma = 1.67$ before to $\sigma = 1.34$ after the coating event.

The compaction can also be expressed in terms of fractal dimensions of the Diesel soot particles before and after the coating event: the COSIMA model calculates an increase of the fractal dimension from $D=1.9$ to 2.1 upon coating. The value for the initial fractal dimension agrees perfectly with the one reported by Nelson, Crookes, and Simons (1990) and Harris and Maricq (2002), but is lower than found by Weingartner, Burtscher, and Baltensperger (1997) possibly due to the use of different Diesel engine types with different exhaust gas treatment and different operation conditions.

Fig. 9 shows a comparison of COSIMA calculations of aerosol mass, surface, and number concentration with measured values. The parameters used for the COSIMA calculations are summarised in Table 2. The calculation for the uncoated Diesel soot aerosol was initialised 3.6 h before the coating event, assuming $D = 1.9$ as determined from experiment No. 2 (Wentzel, Gorzawski, Naumann, Saathoff, & Weinbruch, 2003). The calculation for the coated Diesel soot was started 3.2 h after adding α -pinene to the aerosol assuming that the coating process was completed. The initial monomer diameter of 22.0 nm was increased with a coating layer of 8.3 to 38.6 nm, assuming that 82% of the low volatile oxidation products had condensed on the surface of the soot particles, see above. The fractal dimension of the compacted soot particles was determined by taking advantage of the fact that the mobility equivalent diameter of a fractal-like cluster is related to its

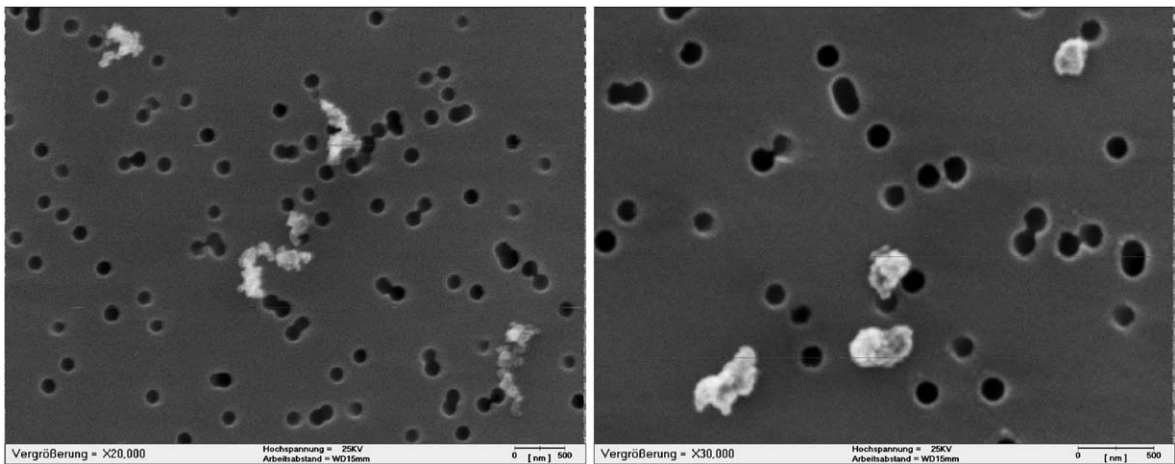


Fig. 8. SEM pictures of Diesel soot before (left) and after coating (right) with α -pinene oxidation products in experiment No. 7.

number of monomers and thus to its mass by a scaling law in terms of D (Naumann, 2003). The mass concentration related to the soot mode of the size distribution was estimated to be $123 \mu\text{g m}^{-3}$ by continuing the COSIMA calculation for the uncoated aerosol to 3.2 h and adding a SOA coating of $53 \mu\text{g m}^{-3}$. Transforming the soot mode of the measured mobility size distribution into a size distribution based on the number of monomers and comparing its average bulk density weighted integral with the estimated mass concentration then uniquely fixes the value of the fractal dimension to $D = 2.1$, leaving no adjustable parameter for the COSIMA simulation.

Fig. 10 shows a 95% decrease of the photoemission signal of Diesel soot compared to the signal before the coating event. This indicates that the SOA coating significantly reduces the probability of photoelectron emission. Also shown in Fig. 10 is the aerosol surface area measured by the diffusion charger (DC). Note that the instrument exhibited a problem: the signal started to decrease each time the instrument was switched from particle-free reference air to aerosol from the AIDA chamber although the surface area of the particles was essentially constant. However, this does not invalidate the following observation: during the coating process the signal increased almost instantaneously by about $2 \text{ cm}^2 \text{ m}^{-3}$. This indicates that the emerging surface area of the nucleation mode overcompensated the loss of Diesel soot surface area due to compaction of the particles. Calculating the surface area from the size distribution measured 35 min after the coating process yields a surface area density of about $9 \text{ cm}^2 \text{ m}^{-3}$ for the nucleation mode. Therefore we estimate an active surface area density loss due to the compaction of the soot agglomerates of about $7 \text{ cm}^2 \text{ m}^{-3}$. This value is perfectly reproduced by the COSIMA simulations.

As shown by Schnaiter et al. (2003), the coated particles scattered more like Mie-type particles and exhibited a strongly enhanced extinction coefficient. Fig. 11 shows furthermore that the coating led to a strong increase of the single scattering albedo from about 0.2 to 0.5, as well as to a change in the wavelength dependence of the scattering coefficient and to a 30% increase of the absorption coefficient. The latter effect has been predicted in model calculations, e.g. by Fuller, et al. (1999), and Jacobson (2001). Aethalometer measurements by Weingartner et al. (2003) are

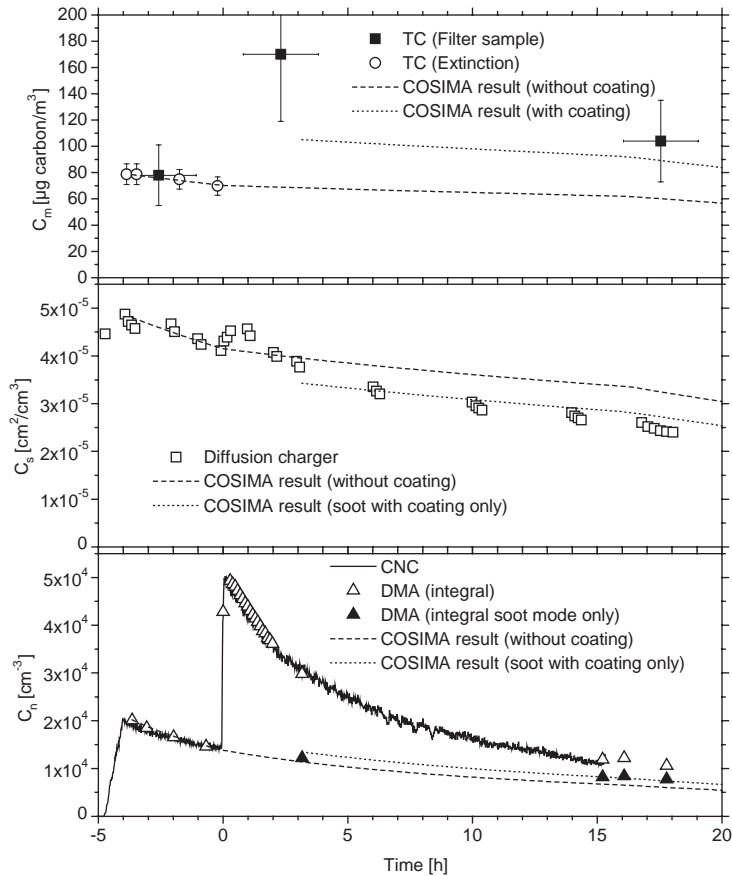


Fig. 9. Evolution of measured aerosol mass, surface, and number concentrations during experiment No. 7 compared to values calculated with the COSIMA model.

Table 2

Parameters used in COSIMA calculations

Exp. No.	Soot type	Fractal dimension	Monomer diameter (nm)	Volume filling factor	Density (g cm^{-3})	Overlap factor
7	Diesel	1.9	22.0	1.05	1.7	0.15
7	Coated Diesel	2.1	36.4	0.36	1.33	0.48
9	“Palas”	2.0	7.3	1.43	2.0	0 ^a
9	Coated “Palas”	2.3	11.0	0.55	1.46	0.34

^aNo overlap of monomers assumed since this parameter is unknown.

also consistent with an absorption increase of the coated Diesel soot particles by 30–40%. The initial rise of the backscatter ratio and of the Angström exponent is attributed to the compaction of the soot agglomerates. This is followed by condensational growth, as evidenced by the subsequent decrease of the backscatter ratio and the Angström exponent.

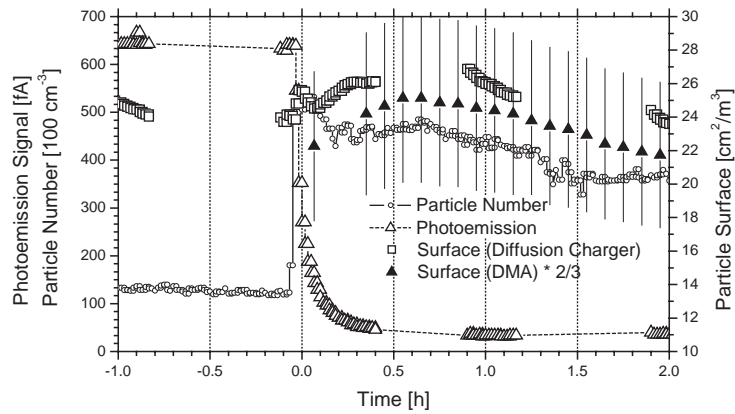


Fig. 10. Evolution of the number concentration, surface area and photoelectric yield during experiment No. 7.

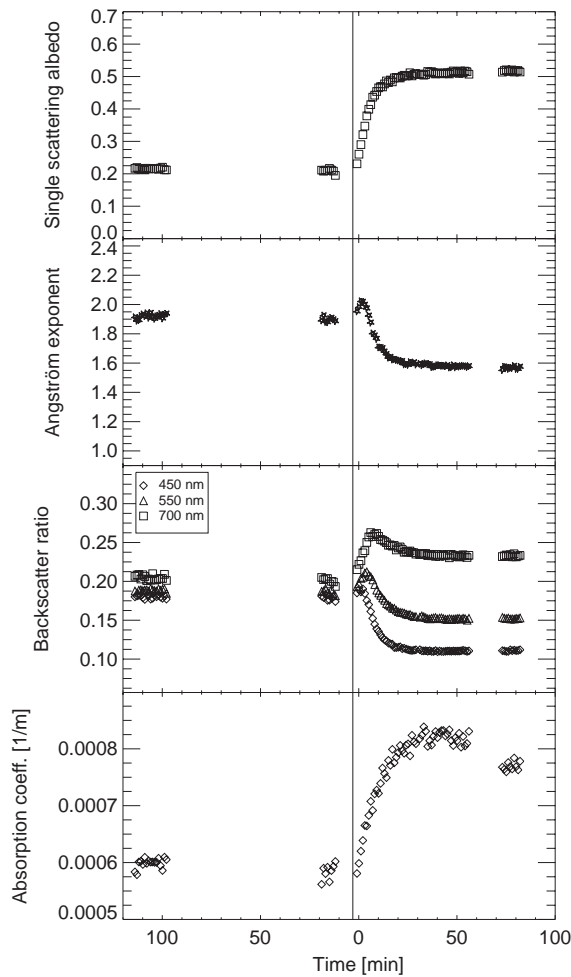


Fig. 11. Evolution of the single scattering albedo, Angström exponent, backscatter ratio, and absorption coefficient of Diesel soot coated by ozonolysis of α -pinene in experiment No. 7.

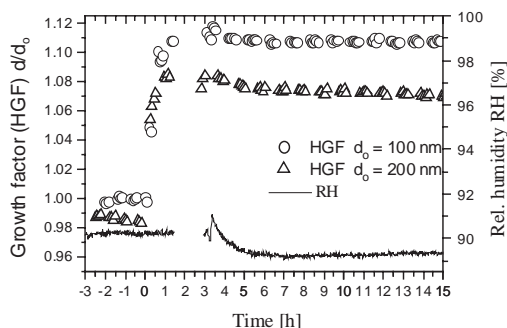


Fig. 12. Hygroscopic growth factor (HGF) of $d_0 = 100$ nm and 200 nm Diesel soot particles vs. ageing time. The coating of the particles starts at $t = 0$. The RH responsible for this growth is also shown and lies between 89.2% and 91%.

The temporal evolution of the measured HGF of uncoated and coated Diesel soot particles at $(89.7 \pm 0.5)\%$ RH are shown in Fig. 12. Uncoated diesel soot particles show a hydrophobic behaviour: 100-nm particles are characterised by no hygroscopic growth, whereas 200-nm particles reduce their diameter by about 1.2%. This is different to findings from another study (Weingartner et al., 1997) where freshly emitted diesel soot particles were characterised by a slight hygroscopic growth ($d/d_0 = 1.01$ for a similar fuel sulphur content). The smaller fractal dimension of the particles used in this study may favour capillary condensation in the cavities of larger aggregates, enhancing the potential for compaction of the particles.

As seen in Fig. 12, the coating of the diesel soot particles leads to a sudden change of their hygroscopic properties. During this experiment the growth factor distribution at $t > 0$ remained monomodal. The addition of α -pinene leads to a significant increase of the HGF within the first hour. Particles with $d_0 = 100$ nm showed a HGF of 1.11 at $\text{RH} = 90\%$. Since the number concentration of the 100 nm size fraction is dominated by homogeneously nucleated SOA particles (cf. Fig. 7) it is not surprising that the measured HGF is close to the value for the pure SOA particles ($\text{HGF} = 1.12$ at $\text{RH} = 90.3\%$). Particles with $d_0 = 200$ nm consist mainly of coated diesel soot and showed a HGF of 1.08 at $\text{RH} = 90\%$. This increase is attributed to a reduction of the compaction potential of the dry particles (see above) and the water uptake of the SOA coating.

3.4. Coating of spark generated (“Palas”) soot aerosol

In experiment No. 9 $(111 \pm 34) \mu\text{g C m}^{-3}$ of spark generated “Palas” soot and ~ 500 ppb ozone were present in the AIDA chamber when 61 ppb of α -pinene were added. As can be seen in Fig. 13, and in perfect agreement with the Diesel soot experiment No. 7, the addition of ozone to “Palas” soot aerosol 15 min before the coating event resulted in a 70% decrease of the photoemission signal. However, a small influence of the ozone soot interaction on the hygroscopic and optical properties of the “Palas” soot particles was observed and could clearly be separated from the impact of the coating. Due to the very large surface area density of the “Palas” soot aerosol (Table 1), which exceeded that of experiment No. 7 by at least a factor of three, new particle formation was almost completely suppressed in experiment No. 9, cf. Figs. 13 and 14. Helsper et al. (1993) determined the size of the primary particles to 5 nm and the specific surface area of spark generated soot to $395 \text{ m}^2 \text{ g}^{-1}$

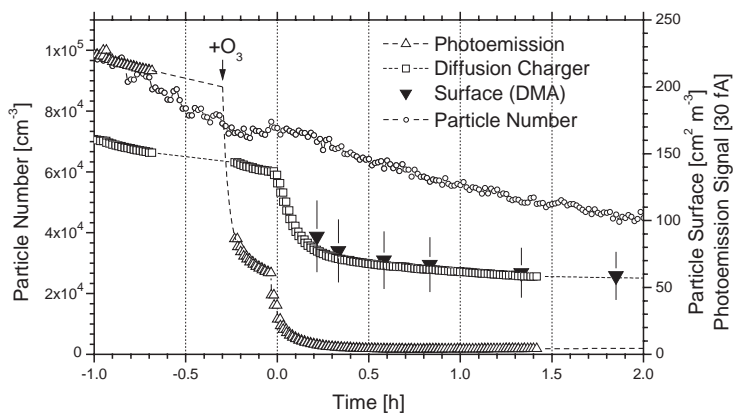


Fig. 13. Evolution of the number concentration, surface area and photoelectric yield during experiment No. 9.

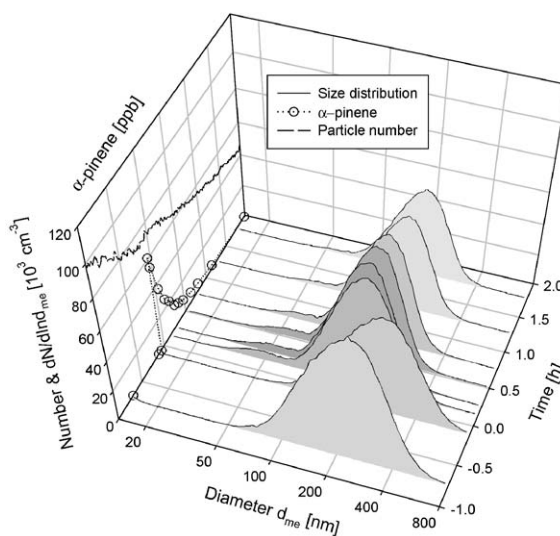


Fig. 14. Evolution of the size distribution and number concentration of “Palas” soot and organic aerosol formed upon ozonolysis of α -pinene in experiment No. 9.

with the BET method. For the “Palas” soot aerosol used in this investigation an average primary particle diameter of 7.3 nm was determined by Wentzel et al. (2003). Kuznetsov, Rakhmanova, Popovitcheva, and Shonia (2003) determined the specific surface area by N_2 thermodesorption/gas chromatography to $(310 \pm 30) \text{ m}^2 \text{ g}^{-1}$. These differences may be due to different operating conditions of the spark discharge generators, which are known to influence the soot particle structure (Schwyn, Garwin, & Schmidt-Ott, 1988).

The active surface area of “Palas” soot was calculated with the COSIMA model (Naumann, 2003) on the basis of the measured size distribution and mass concentration to $150 \text{ m}^2 \text{ g}^{-1}$, cf.

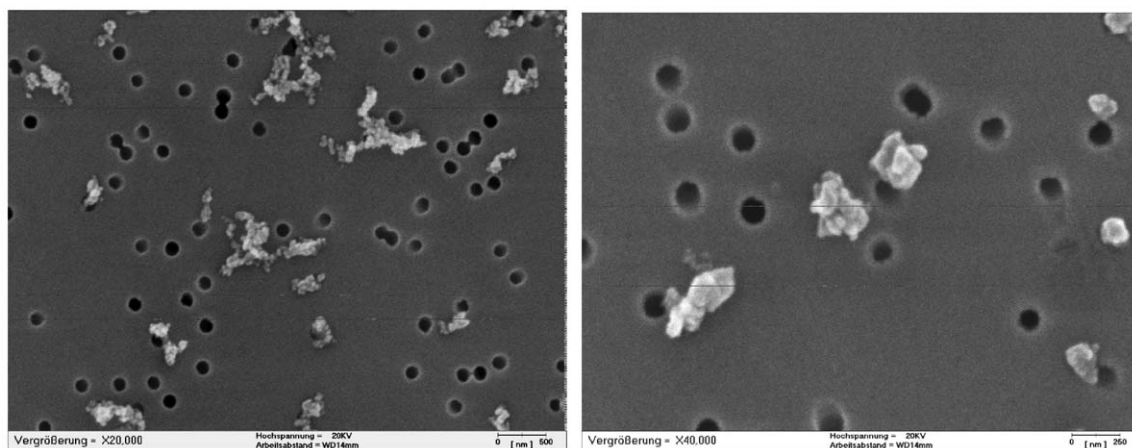


Fig. 15. SEM pictures of “Palas” soot before (left) and after coating (right) with α -pinene oxidation products in experiment No. 9.

Table 1. Thus, the diffusion charger measurements could be calibrated by a factor of about $5.6 \times 10^{-7} \text{ cm}^2 \text{ cm}^{-3} \text{ fA}^{-1}$ for this soot type, very similar to the factor for Diesel soot.

Dramatic changes in most of the measured aerosol parameters were observed when α -pinene was added to the “Palas” soot–ozone mixture. The volume of the extremely weak nucleation mode was negligible in comparison with the expected SOA yield of $65 \times 10^{-6} \text{ cm}^3 \text{ m}^{-3}$ (assumed to be similar as in the two reference experiments Nos. 8 and 10). Condensation of this amount of SOA on the “Palas” soot seed aerosol led to a compaction of the fractal agglomerates, as evidenced by the shift of the “Palas” soot mode from 255 to 175 nm, and a concomitant narrowing of the mode from $\sigma = 1.60$ to 1.40, cf. size distributions shown in Fig. 14. The coating-induced change of the agglomerate structure, which is confirmed by SEM pictures shown in Fig. 15, can also be expressed in terms of fractal dimensions of the “Palas” soot particles before and after the coating event. The COSIMA model calculates an increase of the fractal dimension from 2.0 to 2.3 upon coating.

Fig. 16 shows a comparison of COSIMA calculations of aerosol mass, surface, and number concentration with measured values. The parameters used for the COSIMA calculations are summarised in Table 2. The calculation for the uncoated “Palas” soot was initialised 1.5 h before coating. The calculation for the coated “Palas” soot was started 1.8 h after adding α -pinene to the aerosol, assuming that the coating process was completed. The initial monomer diameter of 7.3 nm was increased with a coating layer of 2.1 to 11.5 nm following the same reasoning as for the Diesel soot coating experiment No. 7. A fractal dimension $D = 2.0$ determined from experiment No. 3 was assigned to the uncoated particles. Its increase to $D = 2.3$ due to agglomerate restructuring was determined in a manner similar to the Diesel soot case. Again there was no adjustable parameter in the COSIMA simulation of the dynamics of the coated particles.

In Fig. 13 a 95% decrease of the photoemission signal of “Palas” soot compared to the value before the coating event can be seen, confirming that the probability of photoelectron emission is significantly reduced by the SOA coating, as previously found for Diesel soot. This is why the

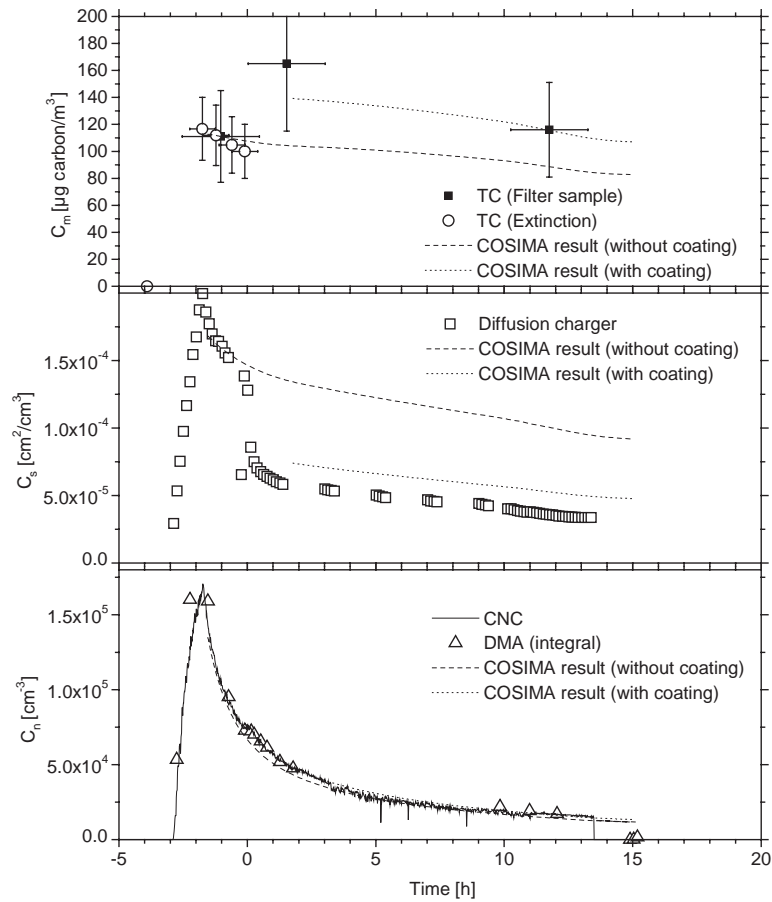


Fig. 16. Evolution of measured aerosol mass, surface, and number concentrations during experiment No. 9 compared to values calculated with the COSIMA model.

usual linear relationship between photoemission signal and diffusion charger signal (Baltensperger et al., 2001) does not hold when the surface properties of soot particles are modified. Fig. 13 shows that the active surface area measured by the diffusion charger decreased from 140 to $60 \text{ cm}^2 \text{ m}^{-3}$, comparable to the value calculated from the measured number size distribution. This is a much stronger decrease in the active surface area than had been estimated for the Diesel soot agglomerates. The result reflects the structural differences of both soot types: spark generated soot agglomerates are composed of many small monomers, while Diesel soot agglomerates consist of less but larger primary particles. For example, considering a mobility equivalent diameter of 200 nm , a Diesel soot particle is estimated to consist of about 200 monomers, and a “Palas” soot agglomerate of about 1900 monomers. These estimates are based on the formalism presented by Naumann (2003), and on the parameters listed in Table 2. Clearly, the fragile structure of “Palas” soot agglomerates gives rise to a much larger compaction potential.

Fig. 17 shows the changes in optical properties induced by coating “Palas” soot aerosol with non-absorbing SOA (Schnaiter et al., 2003). The single scattering albedo increased from about

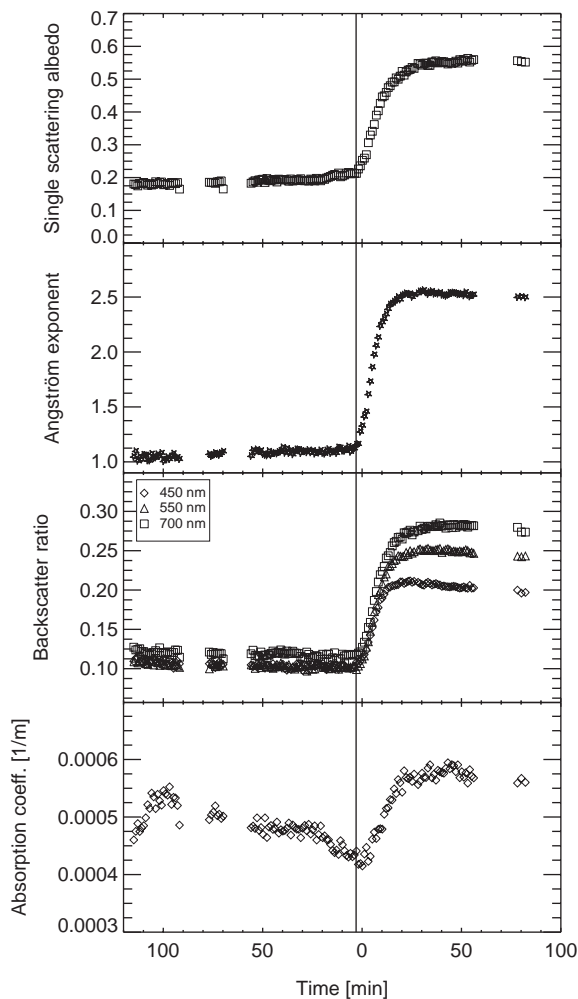


Fig. 17. Evolution of the single scattering albedo, Angström exponent, backscatter ratio, and absorption coefficient of “Palas” soot coated by ozonolysis of α -pinene in experiment No. 9.

0.2 to 0.57 comparable to the Diesel soot experiment No. 7 (Fig. 11). Significant differences are also observed for the backscatter ratio and the Angström exponent. In contrast to experiment No. 7 with Diesel soot aerosol, there is no subsequent drop of the “Palas” soot backscatter ratio or Angström exponent after their strong increase at the onset of the coating process. These differences might be a result of the different compaction properties of the two soot types. Since the Angström exponent depends mainly on the size of the scatterer this behaviour might reflect the ability of partially collapsed “Palas” soot aggregates to absorb larger quantities of supercooled liquid SOA, thus inhibiting substantial growth of the particles by condensation. This interpretation is supported by a wavelength dependent drop of the backscatter ratio observed in the Diesel soot experiment No. 7 (Fig. 11) since scattering of blue light is more size-sensitive than scattering in the red part of the visible spectrum. The differences in the Angström exponent can be interpreted as well by a

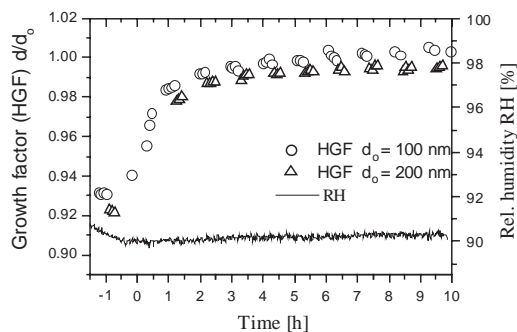


Fig. 18. Temporal evolution of hygroscopic growth factors (HGF) of $d_0 = 100$ and 200 nm “Palas” soot particle (left axis). The coating of the particles starts at $t = 0$, and a HGF < 1 is attributed to a shrinking of the particles. The actual RH at the measurement of d is also shown and lies between 89.8% and 90.5% (right axis).

lower compaction and thus an earlier onset of condensational particle growth in case of the Diesel soot coating experiment. Note the different Angström exponents of uncoated Diesel and “Palas” soot aerosols in Figs. 11 and 17, which point towards different optical properties of these materials (Schnaiter et al., 2003). Particle coating increased the absorption coefficient of “Palas” soot aerosol by 30%; comparable to the Diesel soot experiment No. 7. Aethalometer measurements by Weingartner et al. (2003) revealed an increased absorption of 30–60% increasing with decreasing wavelength. An absorption enhancement of a few ten percent for both types of soot due to a thin organic coating is in reasonable agreement with theoretical predictions by Fuller et al. (1999). Further details are reported by Schnaiter et al. (2003).

The structural differences between Diesel and “Palas” soot agglomerates are also seen in different hygroscopic behaviours. Fig. 18 shows the temporal evolution of the measured HGF at $(90.1 \pm 0.4)\%$ RH for uncoated ($t < 0$) and coated ($t > 0$) $d_0 = 100$ and 200 nm “Palas” soot particles. These particles remained internally mixed after the coating. Uncoated “Palas” soot particles experienced a significantly higher restructuring than Diesel soot particles, i.e. particles with $d_0 = 100$ and 200 nm reduced their diameter by 6.8% and 8%, respectively. This behaviour is explained by the fact that “Palas” soot aggregates are composed of more primary particles having a smaller size than Diesel soot aggregates (see above). This provides more cavities for water absorption resulting in a higher restructuring. The magnitude of the observed restructuring agrees well with measurements performed by Weingartner, Baltensperger, and Burtscher (1995), where the restructuring of “Palas” soot particles was investigated over a larger size range, and the size dependence of d/d_0 was attributed to size dependent particle morphology.

The coating of $d_0 = 100$ and 200 nm particles increased the HGF from 0.932 and 0.92 to ~ 1 and ~ 0.95 , respectively. The fact that a growth factor < 1 is measured for coated $d_0 = 200$ nm particles indicates that the compaction potential was not fully exhausted by the SOA coating.

4. Conclusions

The secondary organic aerosol (SOA) yield found in these experiments for the ozonolysis of α -pinene is in reasonable agreement with values reported in the literature. Convincing evidence has

been presented that the coating of fractal soot particles with non-absorbing material, which is one of the dominant ageing processes in the atmosphere, induces important changes of the physical, hygroscopic, and optical properties of the particles: coating leads to a substantial compaction of the fractal soot agglomerates. This enhances sedimentation, but decreases coagulation rates. In our chamber experiments the airborne lifetime of coated Diesel soot aerosol decreased by about one fourth compared to the COSIMA reference calculation for uncoated aggregates. The active surface area of Diesel soot particles was diminished by only about 10%. The deposition of more hygroscopic condensable ozonolysis products of α -pinene on soot agglomerates results in an increase of the growth factor at 90% RH. This increase of the HGF corresponds to $\sim 65\%$ to 95% of the growth of pure SOA particles ($d/d_0 = 1.12$).

Being an extremely strong absorber of sunlight, atmospheric soot aerosol gives rise to significant direct positive climate forcing. According to the results presented in this study, the positive forcing calculated for e.g. external mixtures of non-absorbing material and soot may be significantly modified when the soot particles are coated with transparent material such as SOA mass: apart from increasing the single scattering albedo, particle coating was found to enhance the effective absorption cross section of soot aerosol significantly. The dependence of this important phenomenon on the thickness of the coating will be studied in the near future.

Acknowledgements

We acknowledge the financial support by BMBF under grant (AFS 07AF209) and the valuable technical assistance by Elisabeth Kranz, Georg Scheurig, Niklaus Streit and Rainer Buschbacher.

References

- Alvarado, A., Tuazon, E. C., Aschmann, S. M., Atkinson, R., & Arey, J. (1998). Products of the gas-phase reactions of O(³P) atoms and O₃ with α -pinene and 1,2-dimethyl-1-cyclohexene. *Journal of Geophysical Research*, *103*, 25541–25551.
- Andreae, M. O., & Crutzen, J. (1997). Atmospheric aerosols: Biogeochemical sources and role in atmospheric chemistry. *Science*, *276*, 1052–1058.
- Aschmann, S. M., Reissell, A., Atkinson, R., & Arey, J. (1998). Products of the gas phase reactions of the OH radical with α - and β -pinene in the presence of NO. *Journal of Geophysical Research*, *103*, 25553–25561.
- Atkinson, R. (1997). Gas-phase tropospheric chemistry of volatile organic compounds: 1. Alkanes and alkenes. *Journal of Physical and Chemical Reference Data*, *26*, 215–290.
- Baltensperger, U., Weingartner, E., Burtscher, H., & Keskinen, J. (2001). Dynamic mass and surface area measurements. In: K. Willeke, & P.A. Baron, *Aerosol measurement: Principles, techniques and applications* (2nd ed.) Chichester, New York. Wiley.
- Barthelme, R. J., & Pryor, S. (1999). A model mechanism to describe oxidation of monoterpenes leading to secondary organic aerosol 1. α -pinene and β -pinene. *Journal of Geophysical Research*, *104*, 23657–23699.
- Burtscher, H. (1992). Measurement and characteristics of combustion aerosols with special consideration of photoelectric charging and charging by flame ions. *Journal of Aerosol Science*, *23*, 549–595.
- Burtscher, H., & Siegmann, H. C. (1994). Monitoring PAH-emissions from combustion processes by photoelectric charging. *Combustion Science and Technology*, *101*, 327–332.
- Calogirou, A., Larsen, B. R., & Kotzias, D. (1999). Gas-phase terpene oxidation products: A review. *Atmospheric Environment*, *33*, 1423–1439.

- Choi, M. Y., & Chan, C. K. (2002). The effects of organic species on the hygroscopic behaviors of inorganic aerosols. *Environmental Science and Technology*, *36*, 2422–2428.
- Christoffersen, T. S., Hjorth, J., Horie, O., Jensen, N. R., Kotzias, D., Molander, L. L., Neeb, P., Ruppert, L., Winterhalter, R., Virkkula, A., Wirtz, K., & Larsen, B. R. (1998). Cis-pinic acid, a possible precursor for Organic aerosol formation from ozonolysis of α -pinene. *Atmospheric Environment*, *32*, 1657–1661.
- Cocker III, D. R., Clegg, S. L., Flagan, R. C., & Seinfeld, J. H. (2001). The effect of water on gas-particle partitioning of secondary organic aerosol. Part I: α -pinene/ozone system. *Atmospheric Environment*, *35*, 6049–6072.
- Cruz, C. N., & Pandis, S. N. (2000). Deliquescence and hygroscopic growth of mixed inorganic-organic atmospheric aerosol. *Environmental Science and Technology*, *34*, 4313–4319.
- Fehsenfeld, F., Calvert, J., Fall, R., Goldan, P., Guenther, A. B., Hewitt, C. N., Lamb, B., Liu, S., Trainer, M., Westberg, H., & Zimmerman, P. (1992). Emissions of volatile organic compounds from vegetation and the implications for atmospheric chemistry. *Global Biogeochemical Cycles*, *6*, 389–430.
- Fuller, K. A., Malm, W. C., & Kreidenweis, S. M. (1999). Effects of mixing on extinction by carbonaceous particles. *Journal of Geophysical Research*, *104*, 15,941–15,954.
- Geron, C., Rasmussen, R., Arnsts, R. R., & Guenther, A. (2000). A review and synthesis of monoterpene speciation from forests in the United States. *Atmospheric Environment*, *34*, 1761–1781.
- Glasius, M., Lahaniati, M., Calogirou, A., Di Bella, D., Jensen, N. R., Hjorth, J., Kotzias, D., & Larsen, B. R. (2000). Carboxylic acids in secondary aerosols from oxidation of cyclic monoterpenes by ozone. *Environmental Science and Technology*, *34*, 1001–1010.
- Griffin, R. J., Cocker III, D. R., Flagan, R. C., & Seinfeld, J. H. (1999a). Organic aerosol formation from the oxidation of biogenic hydrocarbons. *Journal of Geophysical Research*, *104*, 3555–3567.
- Griffin, R. J., Cocker III, D. R., Seinfeld, J. H., & Dabdub, D. (1999b). Estimate of global atmospheric organic aerosol from oxidation of biogenic hydrocarbons. *Geophysical Research Letters*, *26*, 2721–2724.
- Guenther, A., Hewitt, C. N., Erickson, D., Fall, R., Geron, C., Graedel, T., Harley, P., Klinger, L., Lerdau, M., McKay, W. A., Pierce, T., Scholes, B., Steinbrecher, R., Tallamraju, R., Taylor, J., & Zimmerman, P. (1995). A global model of natural volatile organic compound emissions. *Journal of Geophysical Research*, *100*, 8873–8892.
- Gysel, M., Weingartner, E., & Baltensperger, U. (2002). Hygroscopicity of aerosol particles at low temperatures. 2. Theoretical and experimental hygroscopic properties of laboratory generated aerosols. *Environmental Science and Technology*, *36*, 63–68.
- Harris, S. J., & Maricq, M. M. (2002). The role of fragmentation in defining the signature size distribution of diesel soot. *Aerosol Science*, *33*, 935–942.
- Hatakeyama, S., Izumi, K., Fukuyama, T., & Akimoto, H. (1989). Reactions of ozone with α -pinene and β -pinene in air: Yields of gaseous and particulate products. *Journal of Geophysical Research*, *94*, 13013–13024.
- Helsper, C., Mölter, W., Löffler, F., Wadenpohl, C., Kaufmann, S., & Wenninger, G. (1993). Investigation of a new aerosol generator for the production of carbon aggregate particles. *Atmospheric Environment*, *27A*, 1271.
- Hoffmann, T., Bandur, R., Marggraf, U., & Linscheid, M. (1998). Molecular composition of organic aerosols formed in the α -pinene/O₃ reaction: Implications for new particle formation processes. *Journal of Geophysical Research*, *103*, 25569–25578.
- Hoffmann, T., Odum, J. R., Bowman, F., Collins, D., Klockow, D., Flagan, R. C., & Seinfeld, J. H. (1997). Formation of organic aerosols from the oxidation of biogenic hydrocarbons. *Journal of Atmospheric Chemistry*, *26*, 189–222.
- Horvath, H. (1997). Experimental calibration of aerosol light absorption measurements using the integrating plate method—Summary of the data. *Journal of Aerosol Science*, *28*, 1149–1161.
- Jacobson, M. Z. (2001). Strong radiative heating due to the mixing state of black carbon in atmospheric aerosols. *Nature*, *409*(8), 695–697.
- Jenkin, M. E., Schallcross, D. E., & Harvey, J. N. (2000). Development and application of a possible mechanism for generation of cis-pinic acid from the ozonolysis of α - and β -pinene. *Atmospheric Environment*, *34*, 2837–2850.
- Kamens, R., Jang, M., Chien, C.-J., & Leach, K. (1999). Aerosol formation from the reaction of α -pinene and ozone using a gas-phase kinetics-aerosol partitioning model. *Environmental Science and Technology*, *33*, 1430–1438.
- Kanakidou, M., Tsigaridis, K., Dentener, F. J., & Crutzen, P. J. (2000). Human-activity-enhanced formation of organic aerosols by biogenic hydrocarbon oxidation. *Journal of Geophysical Research*, *105*, 9243–9254.
- Khamaganov, V. G., & Hites, R. A. (2001). Rate constants for the gas-phase reactions of ozone with isopren, α -, β -pinene, and limonene as a function of temperature. *Journal of Physical Chemistry*, *105*, 815–822.

- Kirchner, U., Vogt, R., Natzeck, C., & Goschnick, J. (2003). Single particle MS, SNMS, SIMS, XPS, and FTIR spectroscopic analysis of soot particles during the AIDA campaign. *Journal of Aerosol Science*, *34*, 1323–1346.
- Kittelson, D. B. (1998). Engines and nanoparticles: A review. *Journal of Aerosol Science*, *29*, 575–588.
- Koch, S., Winterhalter, R., Uherek, E., Koloff, A., Neeb, P., & Moortgat, G. K. (2000). Formation of new particles in the gas-phase ozonolysis of monoterpenes. *Atmospheric Environment*, *34*, 4031–4042.
- Kückelmann, U., Warscheid, B., & Hoffmann, T. (2000). On-line characterization of organic aerosols formed from biogenic precursors using atmospheric pressure chemical ionization mass spectrometry. *Analytical Chemistry*, *72*, 1905–1912.
- Kuznetsov, B. V., Rakhmanova, T. A., Popovitcheva, O. B., & Shonia, N. K. (2003). Water adsorption and energetic properties of spark discharge soot: Specific features of hydrophilicity. *Journal of Aerosol Science*, *34*, 1465–1479.
- Lavanchy, V. M. H., Gäggeler, H. W., Nyeki, S., & Baltensperger, U. (1999). Elemental carbon (EC) and black carbon (BC) measurements with a thermal method and an aethalometer at the high-alpine research station Jungfraujoch. *Atmospheric Environment*, *33*, 2759–2769.
- Leach, K. B., Kamens, R. M., Strommen, M. R., & Jang, M. (1999). Partitioning of semivolatile organic compounds in the presence of a secondary organic aerosol in a controlled atmosphere. *Journal of Atmospheric Chemistry*, *33*, 241–264.
- Lide, D. R. (Ed.), 1999. *CRC handbook of chemistry and physics*. Cleveland, Ohio: Chemical Rubber Company (CRC) Press.
- Lightstone, J. M., Onasch, T. B., Imre, D., & Oatis, S. (2000). Deliquescence, efflorescence, and water activity in ammonium nitrate and mixed ammonium nitrate/succinic acid microparticles. *Journal of Physical Chemistry A*, *104*, 9337–9346.
- Lioussé, C., Cachier, H., & Jennings, S. G. (1993). Optical and thermal measurements of black carbon aerosol content in different environments: variation of the specific attenuation cross-section, Sigma (σ). *Atmospheric Environment*, *27A*, 1203–1211.
- Lioussé, C., Devaux, C., Dulac, F., & Cachier, H. (1995). Ageing of savanna biomass burning aerosols: Consequences on their optical properties. *Journal of Atmospheric Chemistry*, *22*, 1–17.
- Lioussé, C., Penner, J. E., Chuang, C., Walton, J. J., Eddleman, H., & Cachier, H. (1996). A global three-dimensional model study of carbonaceous aerosols. *Journal of Geophysical Research*, *101*, 19411–19432.
- Matter, U., Siegmann, H. C., & Burtscher, H. (1999). Dynamic field measurement of submicron particles from diesel engines. *Environmental Science and Technology*, *33*, 1946–1952.
- Mueller, J. F. (1992). Geographical distribution and seasonal variation of surface emissions and deposition velocities of atmospheric trace gases. *Journal of Geophysical Research*, *93*, 3787–3804.
- Naumann, K.-H. (2003). COSIMA—a computer program simulating the dynamics of fractal aerosols. *Journal of Aerosol Science*, *34*, 1371–1397.
- Naumann, K.-H., & Bunz, H. (1992). Computer simulations on the dynamics of fractal aerosols. *Journal of Aerosol Science*, *23*, 361–364.
- Nelson, J. A., Crookes, R. J., & Simons, S. (1990). On obtaining the fractal dimension of a 3D cluster from its projection on a plane—application to smoke agglomerates. *Journal of Physics D: Applied Physics*, *23*, 465–468.
- Novakov, T., & Penner, J. E. (1993). Large contribution of organic aerosols to cloud-condensation-nuclei concentrations. *Nature*, *365*, 823–826.
- Odum, J. R., Hoffmann, T., Bowman, F., Collins, D., Flagan, R. C., & Seinfeld, J. H. (1996). Gas/particle partitioning and secondary organic aerosol yields. *Environmental Science and Technology*, *30*, 2580–2585.
- Pankow, J. F., Seinfeld, J. H., Asher, W. E., & Erdakos, G. B. (2001). Modelling the formation of secondary organic aerosol. 1. Application of the theoretical principles to measurements obtained in the α -pinene/, β -pinene/, sabinene/, Δ^3 -carene/, and cyclohexene/ozone systems. *Environmental Science and Technology*, *35*, 1164–1172.
- Saathoff, H., Möhler, O., Schurath, U., Kamm, S., Dippel, B., & Mihelcic, D. (2003a). The AIDA soot aerosol characterisation campaign 1999. *Journal of Aerosol Science*, *34*, 1277–1296.
- Saathoff, H., Naumann, K.-H., Schnaiter, M., Schöck, W., Weingartner, E., Baltensperger, U., Krämer, L., Bozoki, Z., Pöschl, U., Niessner, R., & Schurath, U. (2003b). Carbon mass determinations during the AIDA soot aerosol campaign 1999. *Journal of Aerosol Science*, *34*, 1399–1420.
- Saxena, P., Hildemann, L., McMurry, P. H., & Seinfeld, J. H. (1995). Organics alter hygroscopic behavior of atmospheric particles. *Journal of Geophysical Research*, *100*, 18755–18770.

- Schnaiter, M., Horvath, H., Möhler, O., Naumann, K.-H., Saathoff, H., & Schöck, O. W. (2003). UV-VIS-NIR spectral optical properties of soot containing aerosols. *Journal of Aerosol Science*, *34*, 1421–1444.
- Schwyn, S., Garwin, E., & Schmidt-Ott, A. (1988). Technical note: Aerosol generation by spark discharge. *Journal of Aerosol Science*, *19*, 639–642.
- Seinfeld, J. H., Erdakos, G. B., Asher, W. E., & Pankow, J. F. (2001). Modelling the formation of secondary organic aerosol (SOA). 2. The predicted effects of relative humidity on aerosol formation in the α -pinene-, β -pinene-, sabinene-, Δ^3 -carene-, and cyclohexene-ozone systems. *Environmental Science and Technology*, *35*, 1806–1817.
- Sheehan, P. E., & Bowman, F. M. (2001). Estimated effects of temperature on secondary aerosol concentrations. *Environmental Science and Technology*, *35*, 2129–2135.
- Shulman, M., Jacobson, M., Charlson, R. J., Synovec, R. E., & Young, T. E. (1996). Dissolution behaviour and surface tension effects of organic compounds in nucleating cloud droplets. *Geophysical Research Letters*, *23*, 277–280.
- Virkkula, A., Van Dingenen, R., Raes, F., & Hjorth, J. (1999). Hygroscopic properties of aerosol formed by oxidation of limonene, alpha-pinene, and beta-pinene. *Journal of Geophysical Research*, *104*, 3569–3579.
- Weingartner, E., Baltensperger, U., & Burtscher, H. (1995). Growth and structural change of combustion aerosols at high relative humidity. *Environmental Science and Technology*, *29*, 2982–2986.
- Weingartner, E., Burtscher, H., & Baltensperger, U. (1997). Hygroscopic properties of carbon and diesel soot particles. *Atmospheric Environment*, *31*, 2311–2327.
- Weingartner, E., Gysel, M., & Baltensperger, U. (2002). Hygroscopicity of aerosol particles at low temperatures. 1. New low-temperature H-TDMA instrument: Setup and first applications. *Environmental Science and Technology*, *36*, 55–62.
- Weingartner, E., Saathoff, H., Schnaiter, M., Streit, N., Bitnar, B., & Baltensperger, B. (2003). Absorption of light by filtered aerosol particles: Determination of the absorption coefficient using the aethalometer. *Journal of Aerosol Science*, *34*, 1445–1463.
- Wentzel, M., Gorzawski, H., Naumann, K.-H., Saathoff, H., & Weinbruch, S. (2003). Transmission electron microscopical and aerosol dynamical characterisation of soot and ammonium sulphate/soot mixtures. *Journal of Aerosol Science*, *34*, 1347–1370.
- Xiong, Y., Pratsinis, S. E., & Weimer, A. W. (1992). Modeling the formation of boron carbide particles in an aerosol flow reactor. *AIChE Journal*, *38*, 1685–1692.
- Yu, J., Cocker III, D. R., Griffin, R. J., Flagan, R. C., & Seinfeld, J. H. (1999). Gas-phase ozone oxidation of monoterpenes: Gaseous and particulate products. *Journal of Atmospheric Chemistry*, *34*, 207–258.